Simultaneous Enhancement of Electrical Conductivity and Thermopower of Bi_2Te_3 by Multifunctionality of Native Defects

Joonki Suh, Kin Man Yu, Deyi Fu, Xinyu Liu, Fan Yang, Jin Fan, David J. Smith, Yong-Hang Zhang, Jacek K. Furdyna, Chris Dames, Wladyslaw Walukiewicz, and Junqiao Wu*

Thermoelectric materials have been heavily investigated over the past several decades for environment-friendly applications of solid-state energy conversion: heat to electricity and vice versa.[1,2] The figure of merit (ZT) of thermoelectric materials is given by $\alpha^2 \sigma T/\kappa$, in which α is the Seebeck coefficient (thermopower), σ is the electrical conductivity, T is absolute temperature, and κ is the thermal conductivity. Since α and σ are anticorrelated through the free carrier concentration (n), recent successes to enhance ZT have mostly relied on reduction of lattice thermal conductivity (κ_l) without significantly affecting the power factor ($\alpha^2 \sigma$).[3] This approach has achieved ZT of PbTe–SrTe compounds exceeding 2 at temperatures above 900 K by effectively scattering acoustic phonons with all-length-scale mean free paths.[4]

On the contrary, the best single-phase materials (i.e., excluding superlattices)[5] available today for near-room-temperature thermoelectrics are Bi_2Te_3-based bulk alloys, and their best ZT is still around 1, e.g., n-type $Bi_2Te_{2.7}Se_{0.3}$ with $ZT_{max} \approx 0.9$[6] and p-type $Bi_{0.5}Sb_{1.5}Te_3$ with $ZT_{max} \approx 1.2$.[7] The approach of phonon engineering has limited potential for these materials as their thermal conductivity is already low and does not have much room for further reduction.[5,8] Hence, it is ultimately necessary to seek a breakthrough in materials engineering that would improve ZT beyond what is limited by the trade-off between α and σ, preferably with a single methodology. Though various experimental (e.g., energy filtering in Bi_2Te_3/Bi_2Se_3 superlattices)[9] and theoretical (e.g., hybridization by topological surface states)[10] approaches have been attempted or proposed, only α or σ, but not both, is effectively improved in these cases. The trade-off between α and σ originates fundamentally from the fact that a high α prefers a large asymmetry in electron population above and below the Fermi level, thus a rapid variation in the material density of states; this is opposite to the direction of increasing σ and n, which occurs typically as the Fermi level is displaced deep into the band where the density of states is relatively constant.

Here, we demonstrate a new way to drastically enhance thermoelectric properties of Bi_2Te_3 by utilizing native defects (NDs). We present a new, atomic-scale mechanism to break the trade-off between α and σ, simultaneously improving both for enhanced ZT. Such a unique combination of electrical and thermoelectric benefits originates from the multifunctionality of native point defects in Bi_2Te_3 acting as electron donors and electron energy filters. The presented results establish the importance of understanding and controlling point defects in thermoelectric materials as a venue to much improve their device performance.

Bi_2Te_3 thin films with a wide range of thicknesses (11 nm to 1 μm) were grown by molecular beam epitaxy (MBE) on semi-insulating GaAs (001) substrates. In **Figure 1**a, the cross-section high-resolution transmission electron microscopy (HRTEM) image shows clean interfaces without amorphous phases, and shows highly parallel quintuple layers (QLs). The crystallinity of the MBE films was further evaluated by X-ray diffraction (XRD) using the Cu Kα1 radiation line (Figure 1b). The XRD pattern clearly shows strong reflections from {003}-type lattice planes. This is a strong indication of the highly c-axis directional growth of the MBE films. The QL thickness was calculated from the XRD data, giving $d_{QL} = 1.014 \pm 0.005$ nm for Bi_2Te_3 that is consistent with the value of 1.016 nm for bulk Bi_2Te_3.[11]

J. Suh, Dr. K. M. Yu, Dr. D. Fu, Dr. W. Walukiewicz, Prof. J. Wu
Department of Materials Science and Engineering
University of California
Berkeley, CA 94720, USA
E-mail: wuj@berkeley.edu
J. Suh, Dr. K. M. Yu, Dr. D. Fu, Dr. W. Walukiewicz, Prof. J. Wu
Materials Sciences Division
Lawrence Berkeley National Laboratory
Berkeley, CA 94720, USA
Dr. X. Liu, Prof. J. K. Furdyna
Department of Physics
University of Notre Dame
Notre Dame, IN 46556, USA
Dr. F. Yang, Prof. C. Dames
Department of Mechanical Engineering
University of California
Berkeley, CA 94720, USA
Dr. J. Fan, Prof. D. J. Smith
Department of Physics
Arizona State University
Tempe, AZ 85287, USA
Prof. Y.-H. Zhang
School of Electrical
Computer and Energy Engineering
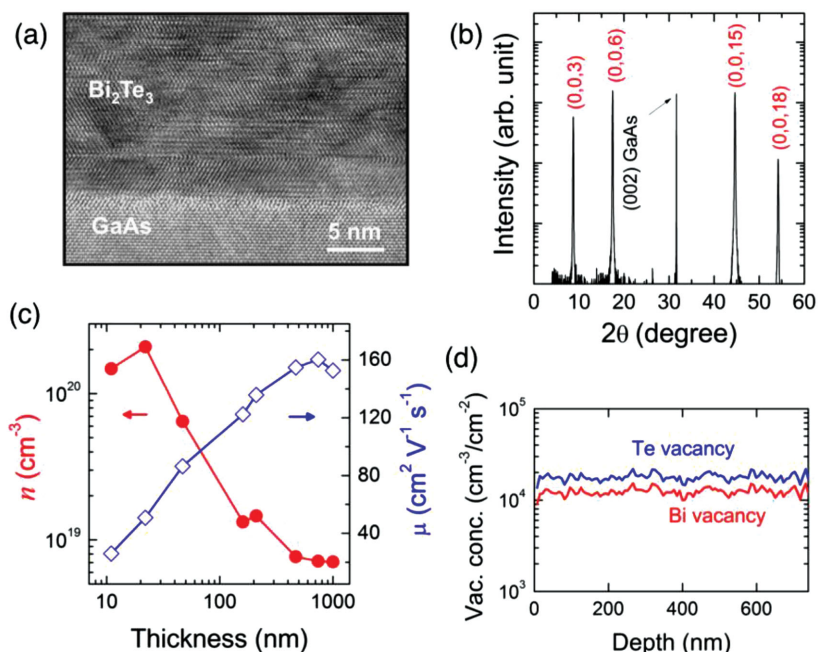Arizona State University
Tempe, AZ 85287, USA

Figure 1. Characterization of pristine Bi_2Te_3 films. a) Cross-sectional HRTEM image and b) XRD data of Bi_2Te_3 films grown by MBE on a GaAs (001) substrate. c) Hall effect determined carrier density and mobility as a function of thickness at room temperature. d) The concentration of vacancies was calculated using SRIM for 740 nm thick Bi_2Te_3 film under 3 MeV alpha particles irradiation. SRIM predicts that the concentration of irradiation-induced defects is very uniform along the depth of films. As indicated by the units (cm^{-3}/cm^{-2}), the real vacancy concentration is given by this value multiplied with the irradiation dose (in units cm^{-2}), implying a linear dependence between them.

Hall effect measurements were performed in the van der Pauw configuration using an Ecopia HMS-3000 system. As presented in Figure 1c, n decreases and carrier mobility (μ) increases monotonically with film thickness, and tends to saturate in thicker films, akin to those observed in Bi_2Se_3 MBE thin films.[12] In order to generate NDs, the samples were irradiated with 3 MeV alpha particles (He^{2+}) with doses ranging from 2×10^{13} to 3×10^{15} cm^{-2}. The projected range of these particles exceeds 8 μm in Bi_2Te_3, as calculated by Monte Carlo simulation using the stopping and range of ions in matter (SRIM) program (Figure S1, Supporting Information, inset). Therefore, the He^{2+} ions completely pass through the entire film thickness, leaving behind NDs that are uniformly distributed in both lateral and depth directions. As predicted by SRIM, the primary NDs induced by irradiation are Bi (V_{Bi}) and Te (V_{Te}) vacancies and corresponding interstitials with average densities of 1.2×10^4 (for Bi) and 1.8×10^4 cm^{-3}/ion cm^{-2} (for Te), respectively, that scale linearly with the irradiation dose (Figure 1d). We note that within the doses used, the materials are gently damaged with only point defects generated; no extended defects, surface sputtering,

non-stoichiometry, or amorphization is observed.[13] We also note that the substrate (semi-insulating GaAs) does not contribute to the electrical conductivity measured from the film. It is theoretically expected[14] and experimentally confirmed that the substrate remains electrically extremely insulating after the irradiation, with a sheet resistance orders of magnitude higher than that of the film.

After the irradiation, σ of the Bi_2Te_3 increases for films with thickness between 47 and 740 nm, and this trend is more significant for thicker films (**Figure 2**a). Considering the multiple conduction channels (e.g., surface and bulk) in Bi_2Te_3, this effect suggests that bulk transport, which is affected by the NDs, plays an important role in the electrical conductance in this thickness range. In contrast, very thin films are insensitive to irradiation, because surface conduction dominates and remains robust to irradiation. Hall effect measurements reveal that the enhanced σ is a combined effect of a monotonic increase in n and a non-monotonic change of μ (Figure 2b,c). The increase in n indicates that the irradiation predominantly introduces donor-like NDs, which are also considered as the primary reason for the unintentional n-type behavior of as-prepared Bi_2Te_3.[15,16]

As shown in Figure 2c, the mobility of thick films increases remarkably (by up to 50%) upon irradiation until an intermediate dose ($\approx 2 \times 10^{14}$ cm^{-2}), then steadily decreases. For
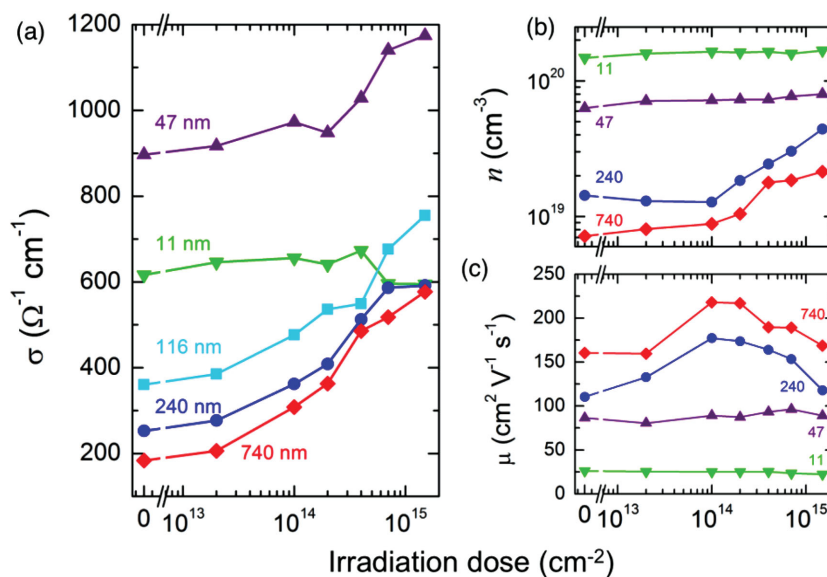

Figure 2. Electrical transport of ND-engineered Bi_2Te_3 thin films. a) Electrical conductivity variation upon irradiation of films with different thicknesses. b) Electron concentration and c) electron mobility of representative Bi_2Te_3 films as a function of irradiation dose, determined by Hall effect measurement at room temperature.
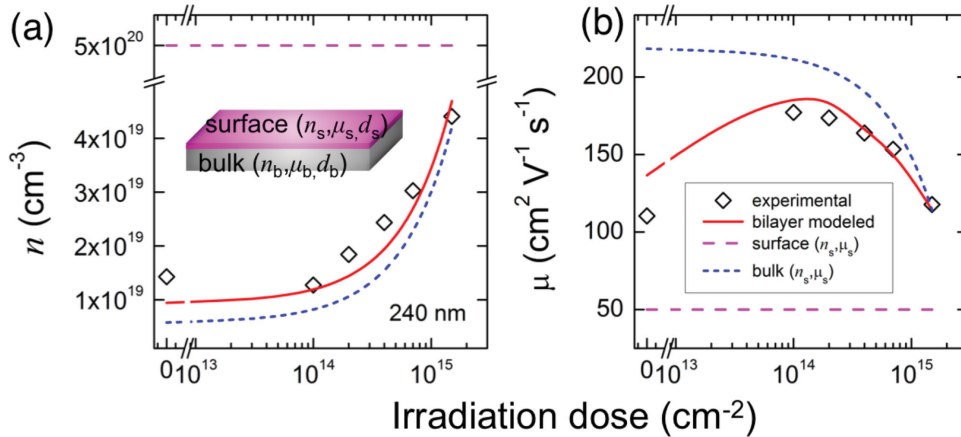
COMMUNICATION

Figure 3. Bilayer Hall effect modeling of Bi_2Te_3 films. Comparison of a) electron concentration and b) electron mobility between experimental data with bilayer modeled data for 240 nm film. Inset shows schematics of the two conduction channels of surface and bulk. Surface properties are assumed to be constant for all the films within the ranges of thickness and irradiation dose. Also, its thickness (d_s) is assumed to be ≈3 nm, considering other contributions such as grain boundaries in the bulk as well as the surface roughness.

conventional semiconductors, it is believed that NDs produced by irradiation are charged Coulomb scattering centers, lowering the carrier relaxation time and thus the carrier mobility. Recent theoretical and experimental studies have shown that in addition to the bulk transport, Bi_2Te_3 exhibits significant surface or grain boundary transport, which are attributed to the topological insulator state[17] or to a surface accumulation layer.[18,19] We propose that the irradiation-induced NDs cause the unusual mobility behavior of Figure 2c by modifying the relative contribution of conduction electrons between the bulk and the surface (including grain boundaries and specimen surface). Simplifying the system into two electrically conduction channels, surface and bulk, we modeled the dependence of carrier concentration and mobility on irradiation dose.[20,21] As illustrated in the inset of **Figure 3**a, parallel electron transport was considered in the surface and bulk layers. With the relative contribution from each layer, effective (modeled) electron concentration (n^*) and mobility (μ^*) were determined using:

$$n^* = \frac{\left[n_s\mu_s(d_s/d) + n_b\mu_b(d_b/d)\right]^2}{n_s\mu_s^2(d_s/d) + n_b\mu_b^2(d_b/d)} \tag{1}$$

$$\mu^* = \frac{n_s\mu_s^2(d_s/d) + n_b\mu_b^2(d_b/d)}{n_s\mu_s(d_s/d) + n_b\mu_b(d_b/d)} \tag{2}$$

where $n_s(n_b)$ and $\mu_s(\mu_b)$ are the electron concentration and mobility of surface (bulk) layer, respectively, and $d_s(d_b)$ is the thickness of surface (bulk) layer, and the total thickness, d, is given by $d = d_s + d_b$.[20] The surface properties (n_s and μ_s) are inferred from Hall effect data of very thin films (11–22 nm) where surface contribution is dominant. Note that in this model n_s and μ_s are assumed to be not strongly affected by irradiation, i.e., the irradiation generates more free electrons only in the bulk (increasing net n_b), as opposed to redistributing existing surface n_s to the bulk n_b. Indeed, in very thin films where the bulk conduction is insignificant, the measured n^* (Hall μ^*) is always dominated by n_s (μ_s), staying high (low) and nearly intact upon irradiation (Figure 2b,c). Given that μ_s is insensitive to the irradiation and $\mu_s \ll \mu_b$,[13,22] n^* and μ^* were fitted to

the experimental Hall effect data at various irradiation doses. Such a bilayer model is in good agreement with the experimental data for films with various thicknesses, explaining both the monotonically increasing n^* and, in particular, non-monotonic variation of μ^* upon irradiation (see representative fitting in Figure 3). The irradiation-induced, drastic net increase in bulk electron density would shift the weight more toward bulk conduction, compared to the case in pristine films where surface conduction weighs more. Therefore, although μ_b slightly decreases upon irradiation, the measured μ^* shows an increase at intermediate irradiation doses, because after irradiation the higher-mobility bulk conduction plays a much more significant role than the surface conduction.

More importantly, while steadily increasing σ, the NDs at intermediate irradiation doses also improve the thermopower (α) of the thick Bi_2Te_3 films as seen in **Figure 4**a. This simultaneous enhancement of α and σ is unusual, since in most cases α decreases and σ increases with increasing n. Normally, as n increases, the Fermi level ε_F moves deeper into the band where the density of states is flatter, hence reducing the entropy carried by charges around ε_F.[23] The simultaneous enhancement of α and σ is observed only in relatively thicker films (>47 nm), which suggests that the measured thermopower is dominated by the bulk contribution that can be tailored by the NDs.

In the relaxation time model, the thermopower in the degenerate doping limit is given by:

$$|\alpha| \approx \frac{k_B}{e} \cdot \frac{\pi^2}{3} \cdot \frac{k_B T}{\varepsilon_F} \cdot \left(\frac{3}{2} + r\right) \tag{3}$$

where r is the index of the electron relaxation time related to kinetic energy, $\tau(\varepsilon) \propto \varepsilon^r$,[24] and ε_F is measured from the conduction band edge. Equation (3) not only predicts the ordinary decrease in α as n increases (through ε_F), but also an increase in α when r increases. The former leads to the conventional wisdom of the inverse coupling between α and σ, while the latter allows it to be broken, as in our case. It is known that r varies from −1/2 for acoustic phonon scattering to 3/2 for ionized impurity scattering.[24] As shown in Figure 4b, in pristine
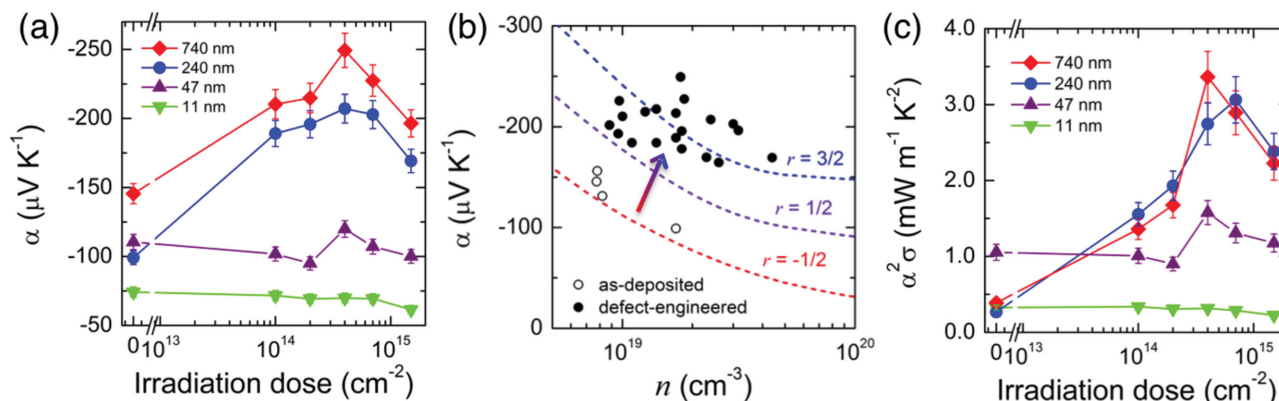
COMMUNICATION

Figure 4. Enhancement of Seebeck coefficient and power factor by the NDs. a) Variation of α upon irradiation. b) α enhancement of irradiated Bi_2Te_3 films in the thick film regime (Pisarenko plot). The dotted lines show the results of calculated Seebeck coefficient with different scattering time index r ranging from phonon-scattering ($-1/2$) to ionized impurity scattering (3/2). Here, the rigorous Fermi–Dirac carrier statistics are used such that the calculation is valid across all concentrations ranging from non-degenerate to degenerate. The arrow indicates simultaneous increase of α and carrier concentration (n) of the films. c) Thermoelectric power factor enhancement in the ND-engineered Bi_2Te_3 films.

films, the measured α as a function of n follows the trend with calculation using $r = -1/2$, indicating that electrons are mostly scattered by phonons in these films. This is consistent with theoretical prediction that electrical transport in Bi_2Te_3 at similar carrier concentrations ($\approx 1 \times 10^{19}$ cm^{-3}) is limited by phonon scattering,[25] and is indeed reasonable considering its very large dielectric constant ($\varepsilon_s = 290$).[26] However, the high density and multiple charge states of NDs introduced by irradiation as ionized impurities cause a transition of the scattering mechanism from phonon-dominated ($r = -1/2$) toward more impurity-dominated ($r = 3/2$); as a result, the thermopower is drastically enhanced, as indicated by the arrows in Figure 4b. For the irradiated films, α starts to follow the calculated trend with $r = 3/2$. This transition is also confirmed by the fact that the mobility μ of the pristine film becomes much higher when measured at low temperatures, while μ is less temperature-sensitive for irradiated films (Figure S1, Supporting Information).

The ND-enabled decoupling of α and σ naturally leads to a significant increase in the thermoelectric power factor, $\alpha^2\sigma$, as shown in Figure 4c. It reaches a peak value of 3.4 ± 0.3 mW m^{-1} K^{-2} for the 740 nm film at an irradiation dose of 4×10^{14} cm^{-2}, representing an eightfold enhancement from its pristine value. This peak power factor is a factor of 1.5–3 higher compared to recently reported values in binary Bi_2Te_3.[9,27]

In addition, the effect of the NDs on the cross-plane (c-axis) thermal conductivity ($\kappa_\perp$), particularly in the thick Bi_2Te_3 films, was investigated using the differential 3ω technique.[28] We found that $\kappa_\perp$ decreases by up to 35% upon the irradiation as shown in **Figure 5**. It is noteworthy that the reduction in $\kappa_\perp$ is substantially stronger than the case if the NDs were replaced by conventional donor ions at the same concentrations ($\approx 3 \times 10^{19}$ cm^{-3}, or $\approx 0.1\%$ of the atomic sites). This is because a point defect's ability to scatter acoustic phonons goes as the square of the defect's relative deviation in mass, radius, and/or bonding strength.[29] These relative deviations are much stronger for the irradiation-introduced NDs (vacancies, antisites, and missing bonds) as compared to simple

substitutional dopants.[30] As our measured κ is cross-plane ($\perp$), while the measured α and σ are in-plane ($//$), a rigorous evaluation of ZT is not within the scope of this work due to the anisotropic transport. However, given the eightfold enhancement in $\alpha^2\sigma$, it is safe to conclude that ZT is expected to be significantly enhanced accordingly, because κ is expected to only decrease upon the irradiation.

To summarize, irradiation-induced NDs drastically enhance thermoelectric properties in Bi_2Te_3 by decoupling the three key thermoelectric parameters and simultaneously modifying all of them toward the desired direction. This is enabled by the multiple functionality of the NDs acting beneficially as electron donors, energy-dependent charge scattering centers, and phonon blockers. Our results suggest that a significant improvement of the thermoelectric performance can
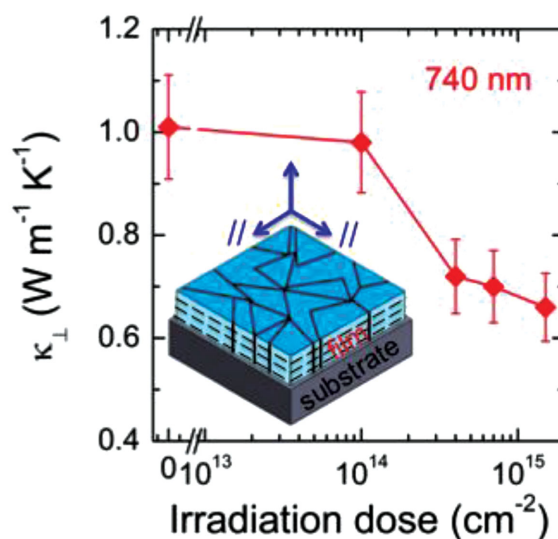

Figure 5. Cross-plane thermal conductivity of the 740 nm Bi_2Te_3 film upon irradiation. Inset illustrates the in-plane and cross-plane configuration of the textured film.

be achieved through a judicious control of the ND species and their density by post-growth processing with high-energy beams. As the NDs are expected to be generated and behave in the similar way in a wide range of narrow-bandgap semiconductors (e.g., observed in InN and InAs)[31,32] it is possible to extend this method to improve the figure of merit of other materials in conjunction with other widely utilized techniques such as alloying and nano- and hetero-structuring. Although irradiation cannot be directly applied to bulk materials due to limitation in irradiation projection range ($\approx$10 μm), our approach is of practical importance because thin film thermoelectrics could play an important role in on-chip cooling;[33] in addition, our approach can be used in complementary to existing nanotechnology to scale up in bulk thermoelectrics. For instance, nano-objects (such as Bi_2Te_3 nanowires, particles, and nanoplates) can be irradiated, and then pressed into bulk or assembled into bulk using a polymer matrix, as demonstrated by Coates et al.[34]

Experimental Section

Thin-Film Growth: The Bi_2Te_3 thin films were grown using a dual chamber Riber 32 solid-source MBE system. The Bi and Te_2 fluxes were generated by standard effusion cells, and the structure and thickness of the films were monitored in situ by reflection high-energy electron diffraction. The growth step was initiated by heating an epi-ready semi-insulating GaAs (001) substrate to 600 °C for de-oxidation in the III-V MBE chamber. This was followed by deposition of a 100 nm GaAs buffer layer. This modified substrate was then transferred to the chalcogenide MBE chamber through an ultra-high vacuum connection. The growth of the MBE film was initiated by the deposition of a series of monolayers of Te–Bi–Te–Bi–Te (a QL) in atomic layer epitaxy fashion at room temperature. The substrate was then gradually heated to 300 °C, and the MBE growth of Bi_2Te_3 was subsequently performed under Te-rich condition of T_{Te} (250 °C) < $T_{substrate}$ (300 °C) < T_{Bi} ($\approx$500 °C) with a Te:Bi beam equivalent pressure ratio ranging from 20:1 to 80:1. The films were grown layer by layer, with typical growth rates of 0.5–2 QL min^{-1}. Later, the compositions and thicknesses of the films were confirmed by Rutherford backscattering spectroscopy (RBS) before further experiments.

Alpha Particle Irradiation: The pristine samples were irradiated in an accumulated manner employing a high-energy (3 MeV) He^{2+} beam with current between 35 and 100 nA generated by an NEC Pelletron tandem accelerator. The accumulated dose was monitored by measuring the total charge on the sample in an electrically isolated irradiation chamber. The ion beam was defocused to an area of 40 mm^2 maintaining a homogeneous ion fluence over the entire film, assuring the introduction of uniformly distributed NDs, both vertically and laterally.

Thermoelectric Transport Characterization: Electrical transport was measured by Hall effect using an Ecopia HMS-3000 system at room temperature. Seebeck coefficient was measured by a home-built thermopower measurement system. A differential 3ω technique was used to measure the cross-sectional thermal conductivity ($\kappa_\perp$) of the ND-engineered Bi_2Te_3 thin film with a thickness of 740 nm at various irradiation doses. Using the plasma-enhanced chemical vapor deposition (PECVD) technique, a 500 nm SiO_2 layer was simultaneously deposited on the top of both a pristine Bi_2Te_3 thin film, for electrical isolation, and a reference (identical semi-insulating GaAs (001)) bare substrate at 300 °C. Two identical 20 μm × 1500 μm gold line heaters were then patterned on the top of PECVD-grown SiO_2 layers using conventional photolithography. Since the thicknesses of the dielectric layer (500 nm) and Bi_2Te_3 film (740 nm) are much thinner than the width of the patterned gold heater (20 μm), the through-thickness (along *c*-axis) heat conduction can be approximated as 1D to better than 5% accuracy.[35]

Supporting Information

Supporting Information is available from the Wiley Online Library or from the author.

[1] S. Chu, A. Majumdar, *Nature* **2012**, *488*, 294.
[2] C. J. Vineis, A. Shakouri, A. Majumdar, M. G. Kanatzidis, *Adv. Mater.* **2010**, *22*, 3970.
[3] A. Shakouri, *Annu. Rev. Mater. Res.* **2011**, *41*, 399.
[4] K. Biswas, J. He, I. D. Blum, C.-I. Wu, T. P. Hogan, D. N. Seidman, V. P. Dravid, M. G. Kanatzidis, *Nature* **2012**, *489*, 414.
[5] R. Venkatasubramanian, E. Siivola, T. Colpitts, B. O'Quinn, *Nature* **2001**, *413*, 597.
[6] X. Yan, B. Poudel, Y. Ma, W. S. Liu, G. Joshi, H. Wang, Y. Lan, D. Wang, G. Chen, Z. F. Ren, *Nano Lett.* **2010**, *10*, 3373.
[7] B. Poudel, Q. Hao, Y. Ma, Y. Lan, A. Minnich, B. Yu, X. Yan, D. Wang, A. Muto, D. Vashaee, X. Chen, J. Liu, M. S. Dresselhaus, G. Chen, Z. Ren, *Science* **2008**, *320*, 634.
[8] J. P. Fleurial, L. Gailliard, R. Triboulet, H. Scherrer, S. Scherrer, *J. Phys. Chem. Sol.* **1988**, *49*, 1237.
[9] Y. Min, J. W. Roh, H. Yang, M. Park, S. I. Kim, S. Hwang, S. M. Lee, K. H. Lee, U. Jeong, *Adv. Mater.* **2013**, *25*, 1425.
[10] P. Ghaemi, R. S. K. Mong, J. E. Moore, *Phys. Rev. Lett.* **2010**, *105*, 166603.
[11] J. O. Jenkins, J. A. Rayne, R. W. Ure, *Phys. Rev. B* **1972**, *5*, 3171.
[12] Y. S. Kim, M. Brahlek, N. Bansal, E. Edrey, G. A. Kapilevich, K. Iida, M. Tanimura, Y. Horibe, S.-W. Cheong, S. Oh, *Phys. Rev. B* **2011**, *84*, 073109.
[13] J. Suh, D. Fu, X. Liu, J. K. Furdyna, K. M. Yu, W. Walukiewicz, J. Wu, *Phys. Rev. B* **2014**, *89*, 115307.
[14] W. Walukiewicz, *Phys. Rev. B* **1988**, *37*, 4760.
[15] D. O. Scanlon, P. D. C. King, R. P. Singh, A. de la Torre, S. M. Walker, G. Balakrishnan, F. Baumberger, C. R. A. Catlow, *Adv. Mater.* **2012**, *24*, 2154.
[16] D. West, Y. Y. Sun, H. Wang, J. Bang, S. B. Zhang, *Phys. Rev. B* **2012**, *86*, 121201(R).
[17] Y. L. Chen, J. G. Analytis, J.-H. Chu, Z. K. Liu, S.-K. Mo, X. L. Qi, H. J. Zhang, D. H. Lu, X. Dai, Z. Fang, S. C. Zhang, I. R. Fisher, Z. Hussain, Z.-X. Shen, *Science* **2009**, *325*, 178.
[18] C. Chen, S. He, H. Weng, W. Zhang, L. Zhao, H. Liu, X. Jia, D. Mou, S. Liu, J. He, Y. Peng, Y. Feng, Z. Xie, G. Liu, X. Dong, J. Zhang, X. Wang, Q. Peng, Z. Wang, S. Zhang, F. Yang, C. Chen, Z. Xu,

COMMUNICATION

X. Dai, Z. Fang, X. J. Zhou, *Proc. Natl. Acad. Sci. USA* **2012**, *109*, 3694.

[19] M. S. Bahramy, P. D. C. King, A. de la Torre, J. Chang, M. Shi, L. Patthey, G. Balakrishnan, Ph. Hofmann, R. Arita, N. Nagaosa, F. Baumberger, *Nat. Commun.* **2012**, *3*, 1159.

[20] R. L. Petritz, *Phys. Rev.* **1958**, *110*, 1254.

[21] R. E. Jones, K. M. Yu, S. X. Li, W. Walukiewicz, J. W. Ager, E. E. Haller, H. Lu, W. J. Schaff, *Phys. Rev. Lett.* **2006**, *96*, 125505.

[22] N. P. Butch, K. Kirshenbaum, P. Syers, A. B. Sushkov, G. S. Jenkins, H. D. Drew, J. Paglione, *Phys. Rev. B* **2010**, *81*, 241301.

[23] H. J. Goldsmid, *Introduction to Thermoelectricity*, Springer, Heidelberg, Germany **2010**.

[24] F. D. Rosi, *Solid-State Electron.* **1968**, *11*, 833.

[25] B.-L. Huang, M. Kaviany, *Phys. Rev. B* **2008**, *77*, 125209.

[26] W. Richter, H. Kohler, C. R. Becker, *Phys. Status Solidi B* **1977**, *84*, 619.

[27] L. Hu, H. Gao, X. Liu, H. Xie, J. Shen, T. Zhu, X. Zhao, *J. Mater. Chem.* **2012**, *22*, 16484.

[28] C. Dames, G. Chen, *Rev. Sci. Instrum.* **2005**, *76*, 124902.

[29] P. G. Klemens, *Proc. Phys. Soc. A* **1955**, *68*, 1113.

[30] A. X. Levander, T. Tong, K. M. Yu, J. Suh, D. Fu, R. Zhang, H. Lu, W. J. Schaff, O. Dubon, W. Walukiewicz, D. G. Cahill, J. Wu, *Appl. Phys. Lett.* **2011**, *98*, 012108.

[31] J. Wu, W. Walukiewicz, K. M. Yu, W. Shan, J. W. Ager, E. E. Haller, H. Lu, W. J. Schaff, W. K. Metzger, S. Kurtz, *J. Appl. Phys.* **2003**, *94*, 6477.

[32] V. N. Brudnyi, N. G. Kolin, A. I. Potapov, *Semiconductors* **2003**, *37*, 390.

[33] I. Chowdhury, R. Prasher, K. Lofgreen, G. Chrysler, S. Narasimhan, R. Mahajan, D. Koester, R. Alley, R. Venkatasubramanian, *Nat. Nanotechnol.* **2009**, *4*, 235.

[34] N. E. Coates, S. K. Yee, B. McCulloch, K. C. See, A. Majumdar, R. A. Segalman, J. J. Urban, *Adv. Mater.* **2013**, *25*, 1629.

[35] T. Borca-Tasciuc, A. R. Kumar, G. Chen, *Rev. Sci. Instrum.* **2001**, *72*, 2139.

ADVANCED MATERIALS

Supporting Information

Simultaneous Enhancement of Electrical Conductivity and Thermopower of Bi_2Te_3 by Multifunctionality of Native Defects

Joonki Suh, Kin Man Yu, Deyi Fu, Xinyu Liu, Fan Yang, Jin Fan, David J. Smith, Yong-Hang Zhang, Jacek K. Furdyna, Chris Dames, Wladyslaw Walukiewicz, and Junqiao Wu*

Supporting Information

Simultaneous Enhancement of Electrical Conductivity and Thermopower of Bi$_2$Te$_3$ by Multi-Functionality of Native Defects

Joonki Suh, Kin Man Yu, Deyi Fu, Xinyu Liu, Fan Yang, Jin Fan, David J. Smith, Yong-Hang Zhang, Jacek K. Furdyna, Chris Dames, Wladyslaw Walukiewicz, and Junqiao Wu*
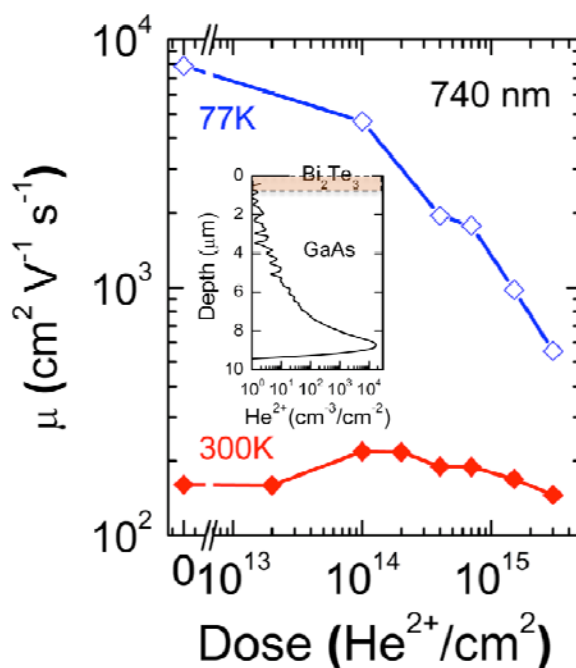
1. Low-temperature mobility.

Figure S1. Low-temperature mobility of Bi$_2$Te$_3$ film. Comparison of carrier mobility determined at 77 K and 300 K for a 740 nm film as a function of irradiation dose. The mobility in the *pristine* film (740 nm thick) at 77 K is nearly two orders of magnitude higher than at 300 K. This difference becomes much smaller upon irradiation, suggesting that electrically active NDs (donors and compensated acceptors), as opposed to acoustic phonons, become the dominant scattering centers, which also increases the Seebeck coefficient. This supports the explanation in the main text of the

simultaneous enhancements in both σ and α. Inset shows the depth distribution of the irradiation

He^{2+} ions in the Bi_2Te_3 film and GaAs substrate determined by SRIM simulation.

2. Thermopower calculation.

The definition of Seebeck coefficient (thermopower), α, can be derived from the solution to the

steady-state Boltzmann transport equation under the relaxation time approximation as[1]

$$\alpha = \frac{2e}{\sigma}\int\frac{d^3k}{(2\pi)^3}\tau(k)\mathbf{v_k}\mathbf{v_k}\frac{\xi}{T}\left(-\frac{df^{(0)}}{d\xi}\right), \tag{S1}$$

where $\sigma = 2e^2\int\frac{d^3k}{(2\pi)^3}\tau(k)\mathbf{v_k}\mathbf{v_k}\left(-\frac{df^{(0)}}{d\xi}\right)$ and $\xi = \varepsilon(k)-(\varepsilon_F - e\phi)$. Here e is the elementary

charge, $\mathbf{v_k}$ is the electron group velocity, ε_F is Fermi energy, φ is electric potential and $f^{(0)}$ is the

Fermi-Dirac carrier distribution function. The dependence of relaxation time τ on electron energy E

follows $\tau(\varepsilon(k)) \sim \varepsilon(k)^r$, where the exponent $r = -1/2$ accounts for phonon dominated scattering

mechanism, while $r = 3/2$ accounts for impurity dominated scattering mechanism. To calculate

Seebeck coefficient as a function of carrier concentration, the Fermi level needs to be determined

first based on the charge neutral condition, i.e.

$$N_d - n(\phi,\varepsilon_F) + p(\phi,\varepsilon_F) = 0, \tag{S2}$$

where N_d is the constant concentration of donors, n and p are the carrier population of the

conduction and valence bands respectively. Setting the conduction band edge as the energy

reference point, i.e. $\varphi = 0$, n can be calculated as

$$n(\varepsilon_F) = \int\frac{\rho(\varepsilon)d\varepsilon}{1+\exp\left[(\varepsilon-\varepsilon_F)/k_BT\right]}, \tag{S3}$$

where $\rho(\varepsilon)$ is the density of states for the conduction band. Here full Fermi-Dirac carrier statistics

are used such that the calculation is valid across all concentrations ranging from non-degenerate to

degenerate. Free hole concentration can be calculated in a similar way. In the degenerate doping limit, Equation (S1) can be simplified to Equation (3) shown in the main text.

3. Characteristics of native defects as charge scattering centers.

Both native defects (NDs) and extrinsic chemical dopants enhance electrical conductivity of Bi_2Te_3 by donating more charge carriers. While they both behave as charged scattering centers, their degree of ionized impurity scattering can be significantly different (hence different effects on Seebeck coefficient).

First, the scattering cross-section is much larger for NDs. For ionized impurity scattering, it is known that the cross-section is proportional to Z^2 as below:

$$\sigma \sim \left[\frac{1}{4\pi\varepsilon\varepsilon_0} \frac{Ze^2}{\frac{1}{2}mv^2} \right]^2, \tag{S4}$$

where Z is the charge of the ionized defect center. It is widely known that NDs in semiconductors have multiple charge states depending on their Fermi level, and this also holds true for Bi_2Te_3 according to a recent computational investigation in Ref [16]. For instance, Te vacancies have the charge state of 2+. Recalling that high-energy particle irradiation normally generates Frenkel pairs (vacancy-interstitial), irradiation-induced NDs can have 4 times larger scattering cross-section compared to that of single charged extrinsic dopants such as iodine (*n*-type) and antimony (*p*-type). Secondly, irradiation-induced NDs provide more charge scattering centers than chemical doping even when they donate the same number of free carriers. This is based on the fact that irradiation produces random damage consisting of donors and compensating acceptors. Although donor-like NDs (e.g., Te vacancies) are dominant, however acceptors (e.g., Bi vacancies) are also simultaneously generated as shown in Figure 1d. Both types of NDs naturally act as charge scattering centers. The carrier scattering rate is given by $1/\tau = Nv\sigma$ where N is the concentration of ionized scattering centers. In compensated semiconductors,

$$N = \frac{n}{Z}\frac{1+\theta}{1-\theta} \ , \tag{S5}$$

where n is free carrier concentration and θ is the effective compensation ratio. For irradiated Bi_2Te_3, θ is estimated to be ~ 0.67 from our SRIM simulation, so N will be ~ 2.5 n. On the contrary, the uncompensated Bi_2Te_3 (e.g., I-doped Bi_2Te_3) will have $N \sim n$. Therefore, our finding of simultaneous enhancements in electrical conductivity and thermopower has never been observed in chemically doped Bi_2Te_3, in which the conventional wisdom of thermoelectrics governs.
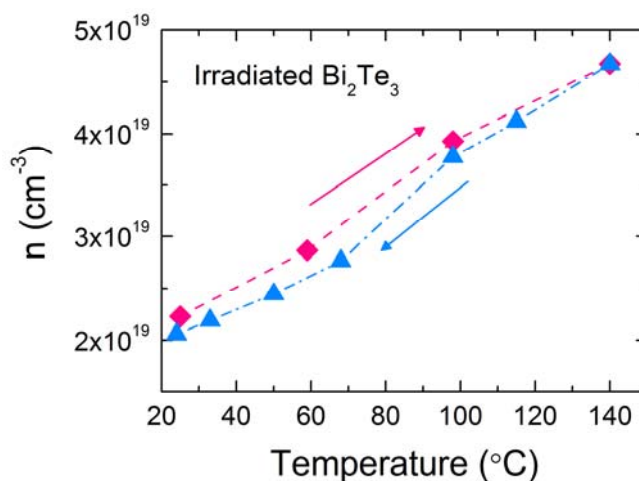
4. Stability of the effects.

Figure S2. Carrier concentration of irradiated Bi_2Te_3 across a practical temperature range. The carrier concentration of 740 nm thin-film was measured during heating (red) and cooling (blue) with a ramping rate of 10 K/min. At each temperature point, the time spent on waiting for temperature stabilization and the Hall measurement is about 10 minutes, such that the total time of a full cycle is about 90 minutes.

5. Reduction of cross-plane thermal conductivity in irradiated Bi_2Te_3.

Figure S3a illustrates these two 3ω samples, namely, "*sample*" (with Bi_2Te_3 film) and "*reference*" (without Bi_2Te_3 film). Figure S3b shows the amplitude of the temperature oscillation in the pristine Bi_2Te_3 sample (ΔT_{sample}) and reference substrate ($\Delta T_{reference}$), calculated using

$$\Delta T = 2R \frac{dT}{dR} \frac{V_{3\omega}}{V_{1\omega}}, \tag{S6}$$

where R, $V_{1\omega}$, $V_{3\omega}$ are the electrical resistance, 1ω voltage, and 3ω voltage of the gold heater, respectively, and dR/RdT is the temperature coefficient of resistance of the heater. The average temperature drop across Bi_2Te_3 film (ΔT_{film}) was determined using $\Delta T_{film} = \Delta T_{sample} - \Delta T_{reference}$, and the cross-plane thermal conductivity of film ($\kappa_{film,\perp}$) was calculated as

$$\kappa_{film,\perp} = \frac{Pd}{Lw\Delta T_{film}}, \tag{S7}$$

where P is the amplitude of the heater power, d is the thickness of film, and L and w are the length and width of the heater, respectively. The representative temperature rise to determine $\kappa_{film,\perp}$ at 1.5×10^{15} cm^{-2} irradiation is shown in Figure S3b. Thermal conductivity was monitored by irradiating both the sample and reference substrate with the same dose. The $R(T)$ curve of every sample and reference was re-calibrated after every additional dosing step. We also note that due to the finite projected range of the alpha particles (see inset of Figure 2a in the main text), the damage profile in the GaAs substrate will be slightly shallower in the "sample" as compared to the "reference" measurements. However, the following estimate shows that this effect should contribute only around 1% of additional uncertainty to the thermal conductivity of the film, and thus is simply neglected. The damaged region of GaAs can be approximated as a layer 1 μm thick that is either ~7 μm (sample) or ~8 μm (reference) below the top GaAs surface. For a comparable point-defect concentration of ~10^{19} cm^{-3}, the thermal conductivity of the damaged GaAs can be estimated as 40 W/m·K, as compared to 60 W/m·K for pristine GaAs. As a conservative estimate of the additional difference between these two samples, we estimate the difference between one-dimensional conduction resistances of 1 μm of damaged and undamaged GaAs, and compare it to the thermal resistance of the 740 nm film at 1 W/m·K. On an area normalized basis this is 8.3×10^{-9} m^{2}K/W compared to 7.4×10^{-7} m^{2}K/W, or only 1.1%.
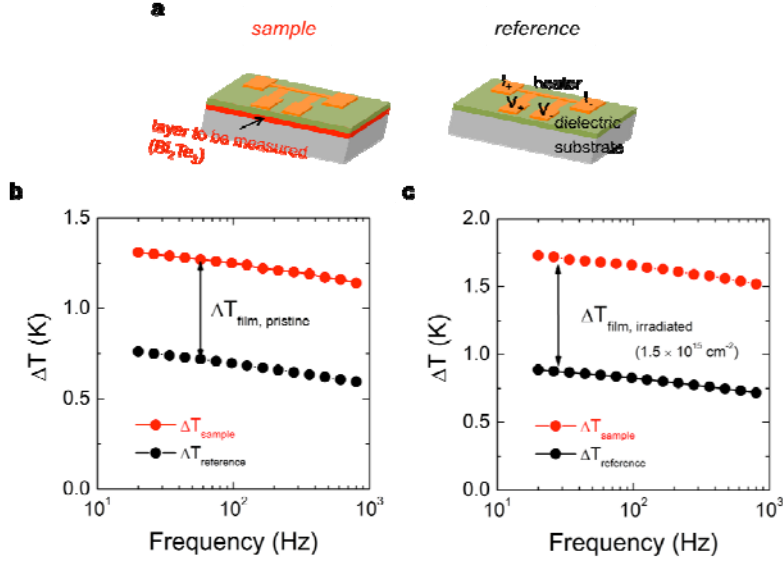
Figure S3. Thermal conductivity of Bi_2Te_3 film. (a) Schematic drawings of two types of specimen used for the differential 3ω measurement: "sample" and "reference". The only difference is the additional Bi_2Te_3 layer in the "sample". Determined temperature rise in the "sample" and "reference" (b) before and (c) after irradiation at a dose of 1.5×10^{15} cm^{-2}. Arrows indicate the temperature rise across the 740 nm Bi_2Te_3 film (ΔT_{film}).

6. Phonon mean free path of Bi_2Te_3.

We first consider the range of phonon mean free paths (MFPs) that are important in bulk Bi_2Te_3 prior to irradiation. The lattice thermal conductivity of a bulk material can be expressed as

$$\kappa_{bulk} = \int \tfrac{1}{3} Cv\Lambda_{bulk}\,d\omega, \tag{S8}$$

where ω is the phonon frequency, C is the volumetric specific heat capacity per unit frequency, v is the group velocity, Λ_{bulk} is the bulk MFP, and each term in the integrand is frequency-dependent. For simplicity we use a Born-von Karman dispersion relation and average the transverse and longitudinal polarizations. Due to its low Debye temperature of 165 K,[2] at 300 K Bi_2Te_3 is well into the Dulong-Petit regime of constant heat capacity. In bulk Bi_2Te_3 of comparable doping,[3,4] Λ_{bulk} at room temperature is dominated by umklapp scattering both in-plane and cross-plane. As a result, $\kappa_{bulk} \propto T^{-1}$, consistent with umklapp-limited transport and inconsistent with other scattering

6

mechanisms such as boundaries and point defects. Thus, the bulk MFP can be approximated as

$\Lambda_{bulk}^{-1} \approx \frac{B\omega^2 T}{v}$,[5] where the free parameter B is determined by substituting this bulk MFP into

Equation (S8) and fitting the model to experimental data for the in-plane[3] and cross-plane[4] lattice

thermal conductivities. The resulting values are $B_{//}$= 4.58×10^{-18} s/K (in-plane) and $B_{\perp}$=1.12×10^{-17}

s/K (cross-plane). The other parameters used in the model are the lattice constants[3] ($a_{//}$ = 0.4383

nm, $a_{\perp}$ = 3.0487 nm) and average sound velocities ($v_{s,//}$ = 2090 m/s, $v_{s,\perp}$ = 2017 m/s).[6]

The resulting accumulation functions[7] for bulk Bi$_2$Te$_3$ at 300 K are shown in Figure S4,

along with typical distribution of grain sizes from ~100 nm to 2 μm in the films. The calculation

shows that the additional scattering by 2 μm grains would have only a modest impact on thermal

conductivity, since 88% (in-plane) and 92% (cross-plane) of κ_{bulk} is carried by phonons with MFPs

shorter than 2 μm. However, for 100 nm grains, effect of grain boundary scattering would be

substantial, and would impact $\kappa_{//}$ more than $\kappa_{\perp}$, since the accumulation function at 100 nm is

smaller in plane (51%) than cross plane (64%). Assuming that the in-plane and cross-plane grain

sizes are similar, this calculation also shows that $\kappa_{//}/\kappa_{\perp}$ should become slightly more isotropic as

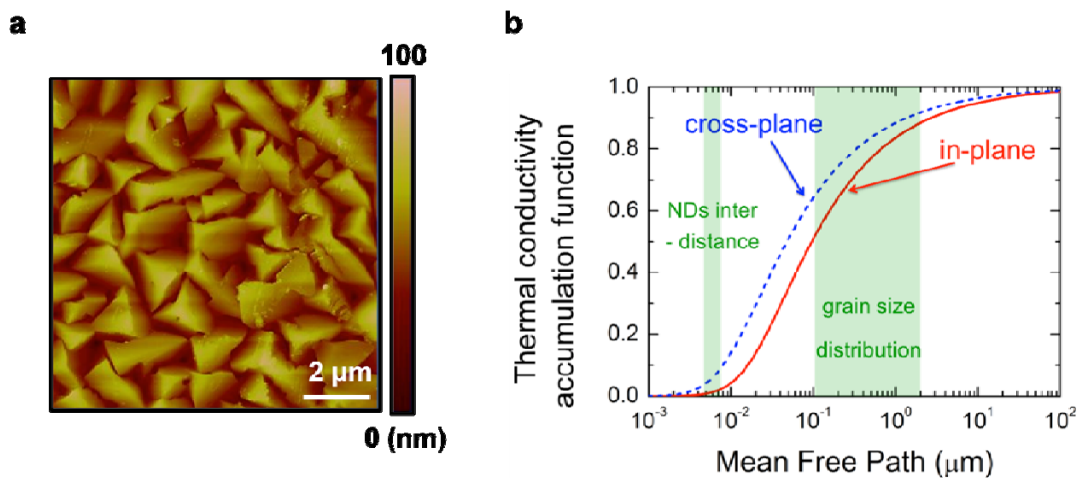grain boundary scattering becomes increasingly important.

Figure S4. (a) AFM image of Bi$_2$Te$_3$ films grown by MBE on a GaAs (001) substrate displaying

grains ranging from 100 nm to 2 μm and oriented in the film plane. (b) Calculated thermal

conductivity accumulation function of non-irradiated Bi_2Te_3. The shaded region represents the range of grain sizes observed in the films.

7. Estimation of bounds of in-plane *ZT*.

As our measured κ is cross-plane ($\perp$) in Figure S3c, while the measured α and σ are in-plane (//), a rigorous evaluation of *ZT* is not within the scope of this work due to the anisotropic transport. For bulk crystalline Bi_2Te_3 at similar carrier concentrations, it is well known that $\sigma_{//}/\sigma_{\perp} \approx 5.0$ and $\kappa_{//}/\kappa_{\perp} \approx 2.0$.[8] Using the Wiedemann-Franz law,[9] the corresponding ratio of phonon thermal conductivities is $\kappa_{//,phonon}/\kappa_{\perp,phonon} \approx 1.7$. As compared to this reference data, the $\kappa_{//}/\kappa_{\perp}$ ratio of the present film samples will differ due to several effects. First, we note that the range of phonon mean free paths (MFPs) of the bulk materials is estimated to span from ~10 nm to ~1 μm, with the MFPs longer in-plane than cross-plane by a factor of ~2. Phonon scattering by grain boundaries affects transport in both directions; but because these grains are textured, $\kappa_{//,phonon}$ should be reduced more than $\kappa_{\perp,phonon}$ due to the longer in-plane MFPs, and it is estimated that about 50% of the in-plane-propagating phonons are scattered at MFPs comparable to the grain sizes in the films (see Figure S4b). Similarly, the strong impurity scattering also tends to reduce $\kappa_{//,phonon}$ more than $\kappa_{\perp,phonon}$, as seen in measurements of Bi_2Te_3[8] and modelling of In_4Se_{3-x}.[10] At the optimal irradiation dose, the NDs distribute over an average distance of ~5 nm, which is much smaller than the median phonon MFP. Overall the $\kappa_{//}/\kappa_{\perp}$ ratio of the 740 nm film should be less than that of single-crystal limit of 2.0.[8] The resulting in-plane *ZT* at room temperature is calculated in Figure S5 for two limiting cases of $\kappa_{//}$. It can be seen that the *ZT* of the optimally irradiated films is at least 0.7 (using the most conservative value of $\kappa_{//}/\kappa_{\perp} = 2.0$), and potentially reaches 1.4 in the isotropic limit ($\kappa_{//}/\kappa_{\perp} = 1.0$). Both values correspond to an enhancement by a factor of ~ 10 in *ZT* compared to the pristine-film values.
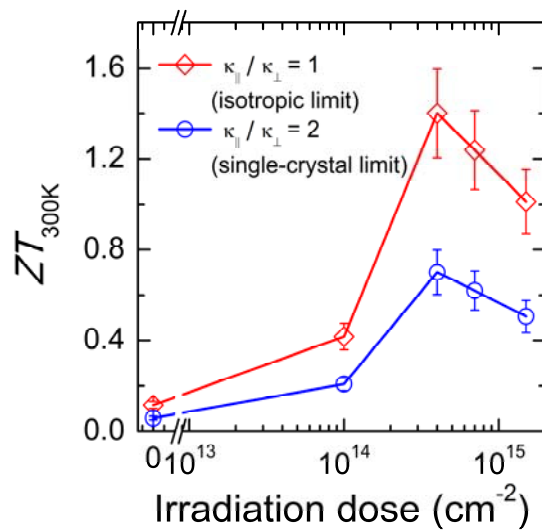
Figure S5. In-plane *ZT* of the irradiated film for anisotropy ratios of 1 (anisotropic, or random polycrystalline limit) and 2 (single-crystal limit), respectively. The real *ZT* value should be in between these two scenarios. In both scenarios the maximum *ZT* is enhanced approximately by an order of magnitude compared to the pristine film.

[1]   J. Cai, G. Mahan, *Phys. Rev. B* **2006**, *74*, 075201.

[2]   O. Madelung, *Semiconductors: Data Handbook,* Springer, **2004**.

[3]   C. B. Satterthwaite, R. W. Ure, *Phys. Rev.* **1957**, *108*, 1164.

[4]   H. J, Goldsmid, *Proc. Phys. Soc. Sec. B* **1956**, *69*, 203.

[5]   F, Yang, T. Ikeda, G. J. Snyder, C. Dames, *J. Appl. Phys.* **2010**, *108*, 034310.

[6]   J. O. Jenkins, J. A. Rayne, R. W. Ure, *Phys. Rev. B* **1972**, *5*, 3171.

[7]   F, Yang, C. Dames, *Phys. Rev. B* **2013**, *87*, 035437.

[8]   H. Scherrer, S. Scherrer, *CRC Handbook of Thermoelectrics.* (eds. Rowe, D. M.) CRC Press, **1995**.

[9]   H. J. Goldsmid, *Proc. Phys. Soc.* **1958**, *72*, 17.

[10]   H. S. Ji, H. Kim, C. Lee, J.-S. Rhyee, M. H. Kim, M. Kaviany, J. H. Shim, *Phys. Rev. B* **2013**, *87*, 125111.